

Wall heat fluxes in enclosure fires

P. Tofilo, M.A. Delichatsios, G.W.H. Silcock and T.J. Shields

*Institute for Fire Safety Engineering Research & Technology(FireSERT), University of
Ulster, Jordanstown BT37 0QG , UK*

Abstract

Even though considerable work has been performed regarding gas temperatures and burning rates in enclosures [1, 2], little information is available for the heat fluxes and their distributions on the walls of an enclosure. These heat fluxes are a necessary input for determining the thermal response of the wall materials and especially glazing. This work develops a mapping of these heat fluxes and generalized scaling relations between the heat flux, the gas temperatures, and mass loss rates with the size of the opening, the size of the fire and the size of the enclosure. The heat fluxes on the wall were deduced from the temperature in several steel plates (25.4 mm x 25.4mm x 3mm thick) and the temperature in the insulation surrounding the steel plates. The enclosure was 1/3 linear scale of the ISO room corner test having six openings and three square- pans of variable size burning IMS (Industrial Methylated Spirits) at the corner and in the center of the enclosure. Further work is planned and under progress to burn methanol and toluene in order to evaluate the effects of sootiness of the fuel on the heat fluxes.

1. Introduction

Prediction of heat fluxes in real fires is an essential and necessary input in determining (a) fire spread and fire growth and (b) the response of non-combustible elements (e.g. steel, concrete, glazing) to the fire. The magnitude of the heat fluxes depends on the sootiness of the burning materials, the size of the fire, the geometry of the enclosure and the burning conditions

(well or under ventilated) inside an enclosure.

Considerable work has been done in this area [1,2] but there is not a definitive and systematic way to determining the heat fluxes either from similarity correlations or from CFD (computational fluid dynamics) calculations. This work attempts to fill some of the gaps in this area by investigating the heat fluxes on the walls of an enclosure from square pan fires burning liquid fuels with different degrees of sootiness such as methanol, IMS (Industrial Methylated Spirits) and toluene.

*Corresponding Author- Tel.: +44-28-903-68573;
E-mail address: p.tofilo@ulster.ac.uk*

One goal is to separate the three main components of this heat flux i.e. radiation from the hot layer, radiation from the flames and convection from the gases around the point of interest. The last component is very important for the estimation of the breakage of glazing because the glazing wholly absorbs convective fluxes, in contrast to radiation fluxes.

The present paper presents only results for the pan fires having the IMS fuel in an enclosure of linear size equal to 1/3 of the ISO room corner and openings of different sizes. The structure of the paper is the following. The experimental setup and procedure are outlined first. A new heat flux gauge using small steel plates surrounded by insulation enables the measurement of heat fluxes on a wall. In combination with a Gardon gauge, the steel plate gauge can yield the convective heat flux. A comprehensive prediction methodology is pursued from the experimental data by (a) correlating the mass pyrolysis rates with the opening factor and the size of the pan [3, 4], (b) correlating the heat flux with the local gas temperature and (c) determining the gas temperature in terms of the heat release rate, the enclosure geometry and the size of the openings.

2. Experimental setup and procedure

Mass loss rates of square pan fires, wall heat fluxes and gas temperatures were measured in an enclosure 1/3 the ISO Room size (0.8m x 1.2m x 0.8m) as shown in Fig. 1. The walls and ceiling had an inner layer 25mm thick insulation board (Fibrefax) and outer layer 10 mm thick of fire retarded chipboard. The floor was made of high density fibreboard.

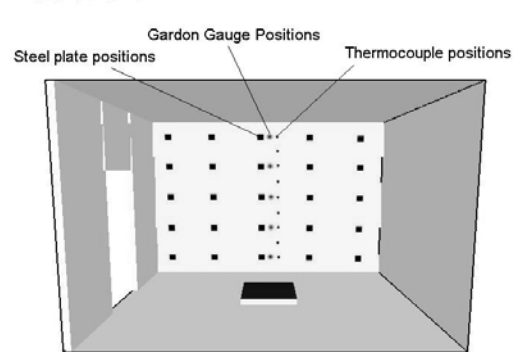


Figure 1. Enclosure and measurement points

The fuel was Industrial Methylated Spirits ,IMS (composition: ethanol 91%, methanol 4%, impurities and water 5%), and burned in square pans of size 0.2 x 0.2m, 0.25 x 0.25m and 0.3 x 0.3m. Each pan was filled with an amount of fuel listed in Fig. 2 and located at the center or corner of the enclosure. The enclosure has an opening of variable size as shown in Fig.2.

Total heat fluxes were measured at twenty five (25) points on one wall (see Fig.1) by using small steel plates whose design and calibration is discussed later. In addition, five Gardon Gauges placed next to the center column of the steel plates measured the heat fluxes. Gas temperatures were measured through a thermocouple tree with nine thermocouples near the instrumented wall; five of these thermocouples were next to the center column of steel plates as illustrated in Fig.1. Data was collected after ignition of the fuel at every four seconds until all fuel was consumed. A new heat flux gauge was developed in this work because mapping of heat fluxes desired over the whole wall area would have been much more costly using commercial Gardon Gauges. A detailed description of the design and calibration is presented in a report for this project [5] and will be published separately. The steel plate has dimensions 25.4 mm x 25.4 mm x 3mm thick and is surrounded by Fibrefax insulation 25 mm thick, as shown in Fig 3.

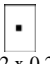









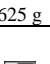

Pan sizes, locations amount of fuel	Openings			
	Shape	Width mm	Height mm	$A_o\sqrt{H_o}$
 0.2 x 0.2 400 g		268	666	0.1456
 0.25 x 0.25 625 g		134	666	0.0728
 0.3 x 0.3 900 g		67	666	0.0364
 0.2 x 0.2 400 g		268	333	0.0514
 0.25 x 0.25 625 g		134	333	0.0257
 0.3 x 0.3 900 g		67	333	0.0128

Figure 2. Openings and pan sizes

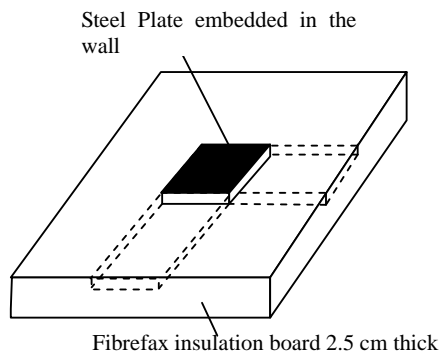


Figure 3. Steel plate surrounded by insulation

The temperature is measured at the center of the unexposed side of steel plate and at two positions in the surrounding insulation, as shown in Fig 4. The front surface of the plate is covered by carbon

black to ensure emissivity one. The heat flux is deduced by accounting for the heat stored in the plate, the radiation losses from the surface, the convection heat transfer at the surface and the conduction heat transfer between steel plates and surrounding insulation.

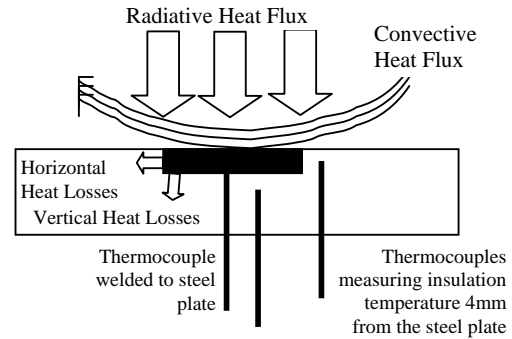


Figure 4. Design and concept of measurement

This design has the advantage over a design where a large plate of steel [6] is used that the lateral conduction losses are reduced, so that heat flux measurement can be reliably made over the whole heating history even if there are large special variations of heat fluxes. In addition, the present device can also be used to deduce the convective heat flux coefficient h_c if the gas temperature T_g next to the plate is also measured. Namely, the convective heat flux coefficient can be evaluated from the measurements of (a) the total heat flux using the Gardon Gauge \dot{q}''_{gardon} (b) the steel plate temperature T_s in nearby locations (c) the nearby gas temperature and (d) the conduction losses to the surrounding insulation deduced from the temperature measurements on the plate and in the surrounding insulation. The relevant relation is :

$$h_c(T_s - T_o) = \dot{q}''_{gardon} - \sigma T_s^4 - \rho c \delta \frac{dT_s}{dt} - \dot{q}''_{cond} \quad (1a)$$

All the quantities in this equation are directly measured or calculated from measured quantities. The plate is thermally

thin of thickness δ ($=3\text{mm}$), density ρ ($=7850 \text{ kg/m}^3$), and specific heat c (temperature dependant $\sim 500 \text{ J/kgK}$). After the heat transfer coefficient is determined at selected locations where both a Gardon gauge and a steel plate are installed, an average value is used for all steel plate locations to obtain the imposed heat flux (referenced to initial temperature of the steel plate) by rearranging Eq.1a as:

$$\dot{q}'' = h_c(T_s - T_o) + \sigma T_s^4 + \rho c \delta \frac{dT_s}{dt} + \dot{q}''_{\text{cond}} \quad (1b)$$

3. Results

Figure 5 depicts and numbers for quick reference the thirty-six experimental conditions of this work using IMS as fuel. Duplicate experiments reproduced nearly the same results. All data is included in a report and is available electronically. As an example, data from the medium pan size fires ($0.25\text{m} \times 0.25\text{m}$) is shown in Figs. 6(a,b,c) and 7 (a,b,c) for the center and the corner fire locations, respectively, and for all opening sizes. Each figure includes the histories for the mass loss, the maximum gas temperature and the maximum heat flux. Two important observations from these figures are:

1. gas temperatures for the fires at the corner are larger than the ones for the fires at the center.
2. a significant increase of the fire intensity is noticeable for the second and third in size opening (see Fig.2) , manifested by larger temperatures, heat fluxes and burning rates in experiments with number 11 and 23 in Fig.6 and with numbers 7 and 19 in Fig.7.

Visual observations and video recordings show that the luminosity of the flames decreased as the size of the opening decreased, presumably mirroring the change of the flames from non-premixed to premixed. This resulted in decrease of the radiation from the flames with concomitant

decrease of the heat fluxes on the instrumented wall.

	1	10	13	22	25	34
	2	11	14	23	26	35
	3	12	15	24	27	36
	5	8	17	20	29	32
	4	7	16	19	28	31
	6	9	18	21	30	33

Figure 5. Matrix of experiments

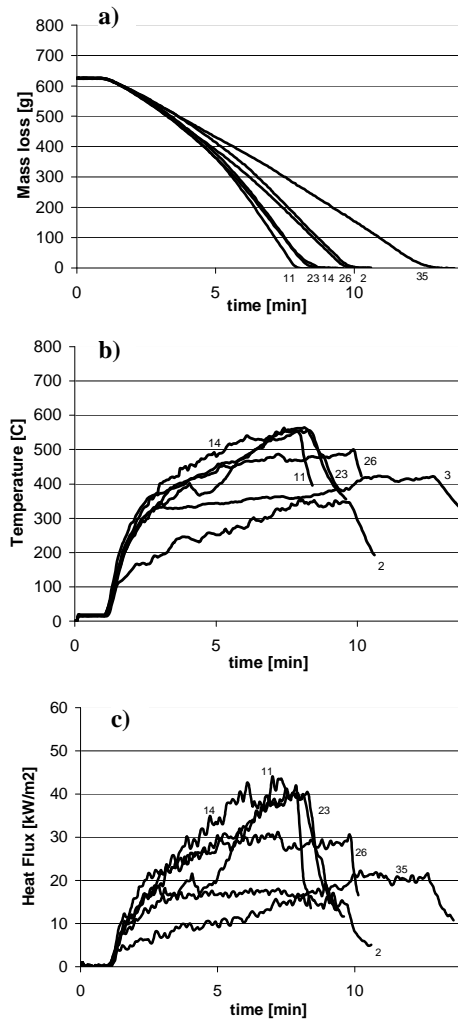


Figure 6 a,b,c. Mass loss, Temperature and Heat flux for centre fires

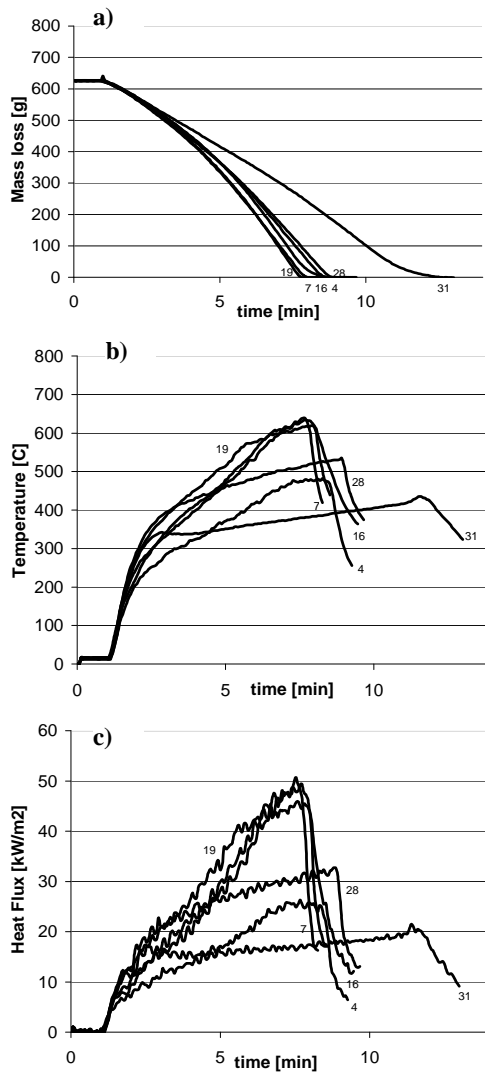


Figure 7 a,b,c. Mass loss, Temperature and Heat flux for corner fires

3. Analysis of experimental results

A comprehensive prediction methodology is pursued from the experimental data by (a) correlating the mass pyrolysis rates with the opening factor and the size of the pan, (b) correlating the heat flux with the local gas temperature and (c) determining the gas temperature in terms of the heat release rate, the enclosure geometry and the size of the openings.

3.1 Mass loss rates for different sizes of pan fires and openings

The mass loss rate derives from differentiation of the mass loss histories (see Figs 6a and 7a). It varies with time but here the maximum mass loss rate is used for analysis that occurs after four minutes from ignition (see Figs.6a and 7a). According to previous work [3,4], the maximum values are normalized by the surface area of the fuel (\dot{m}_{max} / A_F) and plotted in Fig. 8a against the opening factor also normalized by the fuel area ($A_o \sqrt{H_o} / A_F$).

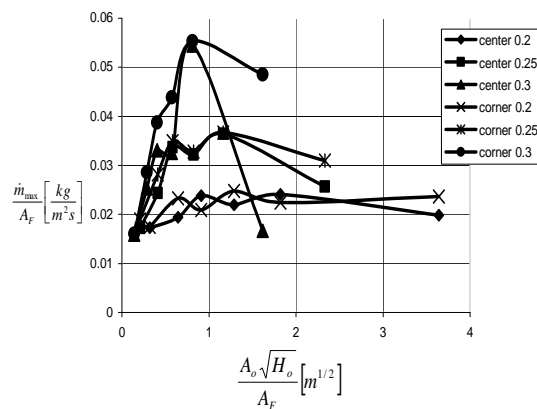


Figure 8a. Normalized mass loss rate per fuel area against normalized ventilation factor per fuel area

It seems, unexpectedly in comparison with the results in [3,4], that the data are grouped according to the pan sizes (surface area of fuel) although they appear to follow the same trends; namely, the normalized mass loss rate increases from a “free” burn to a maximum value before it starts decaying when respectively, the normalized opening factor decreases starting from large values that tend to free burning situations to small values that represent under ventilated situations.

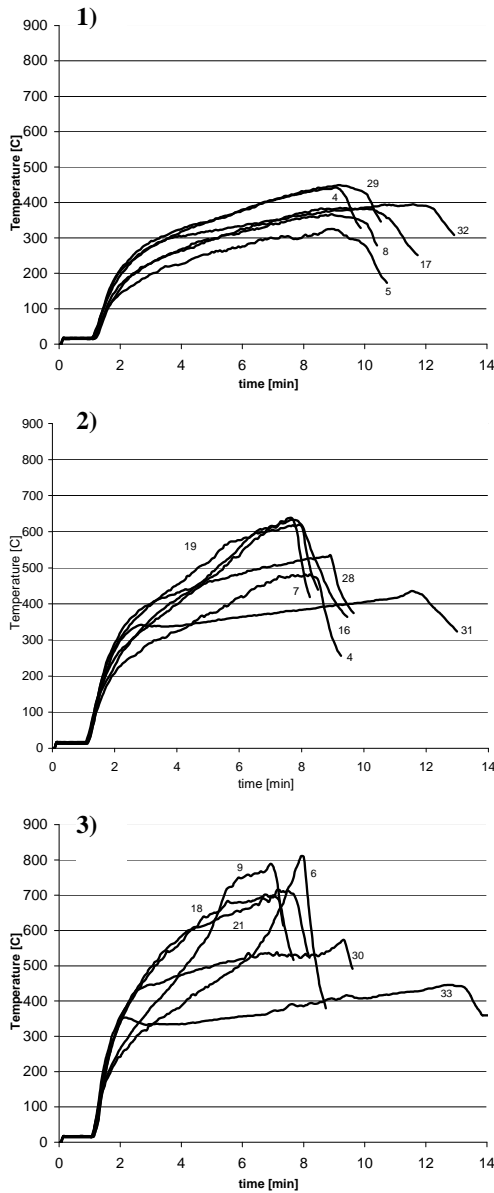


Fig.8b (1,2,3) gas temperature histories for small (0.2 m), medium (0.25 m) and large pans (0.3m)

A clue for the grouping behaviour of the mass loss rate data is found in Fig.8b by inspecting the gas temperatures histories inside the enclosure for the three pan sizes and all the openings. It is seen there that the temperatures become lower for all the openings (large and small) as the size of the pan reduces, probably owing to the increased significance of heat losses for smaller fires. Only the data for the large

pan fire create temperatures high enough for the analysis and correlations in [3,4] to be applicable. Accordingly, in this case the mass loss rate in the under ventilated region is approximately given in Fig 8a by the “classical” relation $\dot{m} = 0.1A_o\sqrt{H_o}$ (units: kg/s, m², m respectively). In contrast, this relation appears to be valid for the smaller pan fires in the under ventilated region but with the coefficient 0.1 decreasing as the pan size decreases. This change in the coefficient may be attributed to the decrease in air inflow in the enclosure if the gas temperature in the enclosure is less than about 400 C as it can be deduced from the Appendix in [4]. The gas temperatures in the enclosure were uniform for under ventilated conditions. The present results and the work in [4] lead to the proposition that the correlation presented in [3,4] is valid only if the gas temperatures in the enclosure is in the range of 600-900 C; for lower temperatures the coefficient in front of the ventilation factor $A_o\sqrt{H_o}$ is decreasing as the gas temperature inside the enclosure also decreases. This is a new result that requires further investigation both experimentally and numerically and cannot be further advanced based on the present data.

For further stimulation, another significant observation emerges also from the data in Fig.8a. Namely, the normalized mass loss rate for well-ventilated fires at the corner tends to its free burning value at a different rate than for well-ventilated fires in the center of the enclosure. This behaviour appears very striking for the large pan fire but still persists for the smaller pan fires.

3.2 Heat fluxes on the walls against gas temperatures in the enclosure

The heat flux imposed on any point at the wall consists of four parts: (a) radiation

from the hot layer (b) convection from the gases at the point of interest (c) radiation from the flames and (d) radiation from hot wall elements. The last part is negligible because the walls were not heated at high temperatures in the present experiments. Thus, the heat flux to any point is, as measured from the steel plate (Eq.1b):

$$\dot{q}'' = \dot{q}''_{rad,hotlayer} + \dot{q}''_c + \dot{q}''_{rad,flames} \quad (2a)$$

The first two terms on the right hand side of this equation depend on the local gas temperature especially if (a) the point is at the upper layer or (b) the fire is ventilation controlled. They can be written as:

$$\dot{q}''_{rad,hotlayer} = \epsilon \sigma T_g^4 \quad (2b)$$

$$\dot{q}''_c = h_c (T_g - T_o) \quad (2c)$$

Here the convective heat flux is referenced at a temperature of the plate equal to its initial temperature (assuming that heat transfer coefficient does not change significantly with the plate temperature). The sum of these terms seems to be mainly dependant on the local temperature.

The last part of the imposed heat flux is the radiation from the flames, which depends on the radiant output of the flames, the distance of the point of interest from the flames and the absorptivity of the gases intervening between the flames and the point of interest. The magnitude of the flame radiation term might be evaluated by comparing heat flux measurements at two points on the wall one close to the other far away from the fire (not done in this work yet).

The previous thoughts and observations are interrogated in Figs. 9(a,b,c) and 10 (a,b,c) which plot the maximum heat fluxes for locations of the fire in the center and in the corner of the enclosure, respectively. More specifically 9a and 10a refer to small, 9b and 10b refer to medium and 9c and 10c refer to large pan sizes. In all these plots, the instantaneous heat flux at a given time is

plotted against the gas temperature at the same time at a location where the heat flux takes its maximum value. The maximum value of the heat flux happens at the highest measurement location at the center of the instrumented wall. In addition, the curve inserted in Figs 9 and 10 depicts the black body radiation flux at a given gas temperature (i.e. σT_g^4). Now, it can be seen from Figs 9a and 10a and Figs 9b and 10b for the small and the medium pan fires that (a) the heat flux depends only on the (local) gas temperature regardless of the location of the fire and (b) the value of these heat fluxes are higher than the black radiation fluxes from the hot gases. The difference is attributed to convective heat flux. This assumption will be also tested in depth by doing the experiments using methanol fuel.

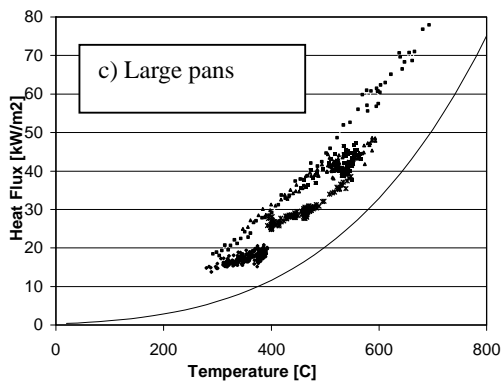
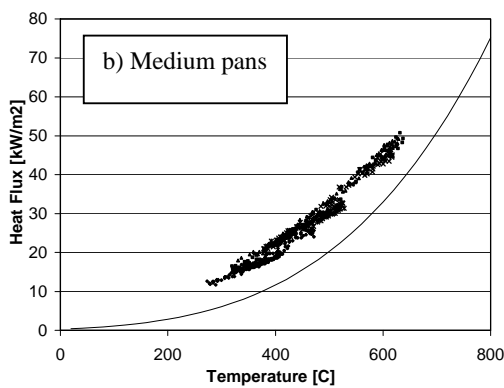
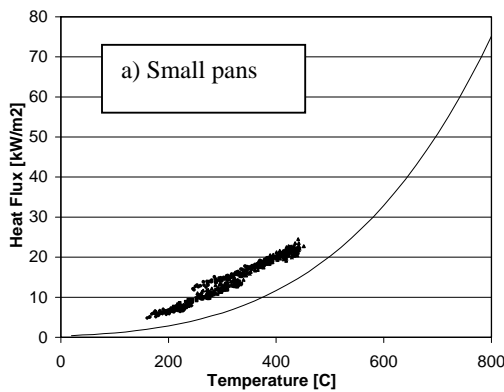
However, the heat flux data in Figs 9c and 10c for the large pan fire emphasize the significance of the flame heat flux which becomes more apparent as the size of the fire increases. This is clearly documented by separating the data for the corner fires of Fig 10c to two plots: (a) one with the smaller openings, Fig.11a and (b) one with the larger openings Fig. 11b. It is evident that as the opening size decreases the curve for the heat flux moves lower because the flames and their radiative heat fluxes become weaker (Fig.5 identifies the parameters of the experiments).

3.3. Correlation of gas temperatures against heat release rates

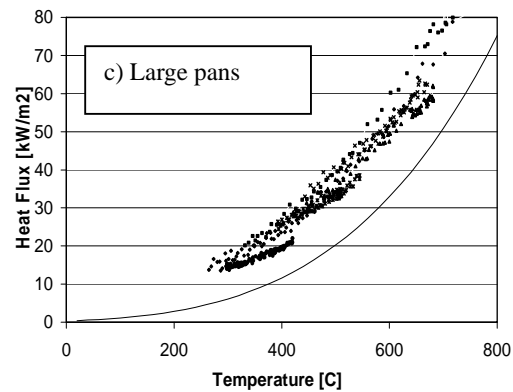
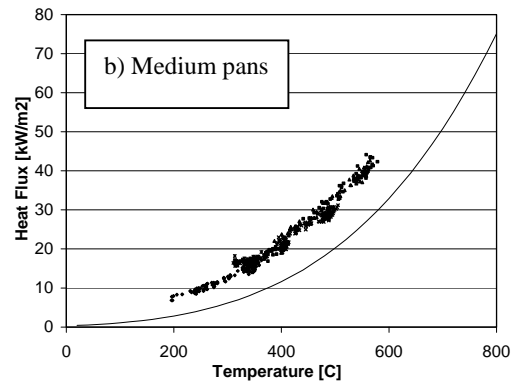
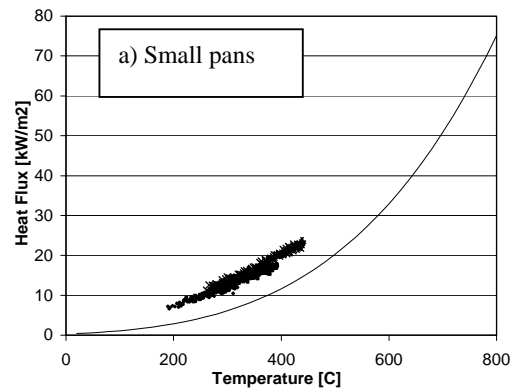
As Figs 9 and 10 manifest, prediction of heat fluxes is possible in many cases (i.e. except if flame radiation is significant) if the gas temperatures near the point of interest are known. These temperatures depend on the size of fire, the enclosure geometry and heat losses through the walls and openings. A well-known correlation MQH (McCarthy-Quintier-Harkleroad)[1,2] for determining the gas temperature proved

not good enough to predict the temperatures in the present experiments. It is also true [1,2] that this correlation leads to a considerable scatter in assessing previous experimental data (see Fig. 6.2 in [2]). A re-examination of the physics related to the development of gas temperature yielded a different correlation, which also includes some of the parameters of the MQH correlation.

Consider the enclosure shown in Fig. 12 with a fire having a small flame height. It is assumed approximately that the interface of the hot layer coincides with the neutral plane. Then, one can equate the entrainment rate into the plume to the flow rate of the hot gases leaving the enclosure. For quasi steady conditions the following relations apply:



Figures 9 a,b,c Heat flux versus temperature for centre fires



Figures 10 a,b,c Heat flux versus temperature for corner fires

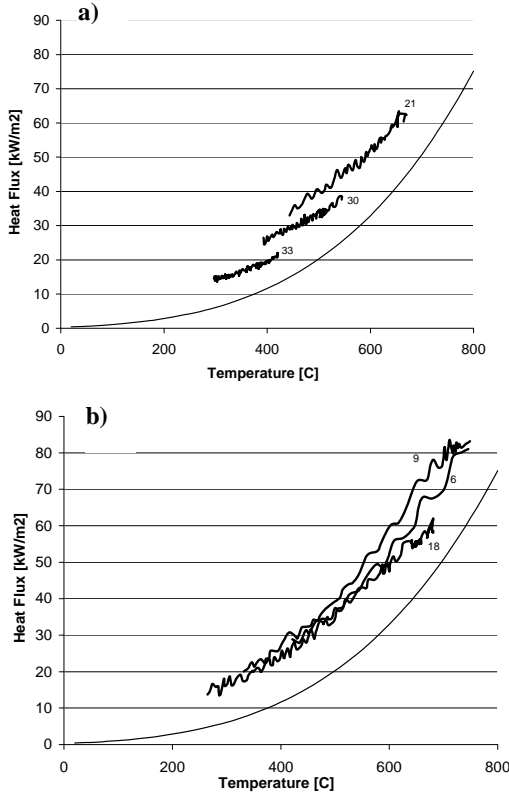


Figure 11a,b. Maximum wall heat flux against temperature for the small (a) and large openings (b) having the large pan at the corner. As the opening size decreases the curve for the heat flux moves lower because the flames and their radiative heat fluxes become weaker (Fig.5 identifies the parameters of the experiments)

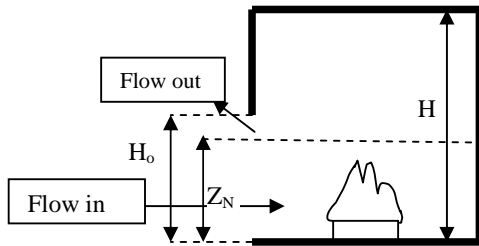


Fig. 12. Schematic of the flow and smoke layer in an enclosure

1. The temperature rise in the gas layer is related to the maximum temperature rise of the fire plume at height Z_N as:

$$\Delta T_f \cong \frac{1}{2} \Delta T_p (1 - \lambda) \quad (3a)$$

where λ is the fraction of heat release representing losses.

2. The entrainment to the plume is:

$$\dot{m}_{\text{plume}} \propto \rho_a \sqrt{\frac{\Delta T_p}{T_a}} Z_N Z_N^2 \quad (3b)$$

3. The flow out of the opening is:

$$\dot{m}_{\text{out}} \propto \rho_a \sqrt{\frac{\Delta T_f}{T_a}} \left(\frac{T_a}{T_f} \right) A_o \sqrt{H_o} \left(1 - \frac{Z_N}{h_o} \right)^2 \quad (3c)$$

Thus equating the plume entrainment with the outflow rate and using Eq.(3a) yields after some algebra:

$$\left(\frac{Z_N}{H_o} \right)^{\frac{5}{2}} \propto \frac{A_o \sqrt{H_o} T_o \sqrt{1-\lambda}}{H_o^{5/2} T_f} \quad (4)$$

This equation has the approximate solution for the height of the interface:

$$\frac{Z_N}{H_o} = \left(\frac{\mu}{1 + \frac{3}{2}\mu} \right)^{\frac{2}{5}} \quad (5a)$$

$$\text{or since } \frac{Z_N}{H_o} < 1 \quad \frac{Z_N}{H_o} \propto \mu^{\frac{2}{5}} \quad (5b)$$

$$\text{where } \mu = \frac{A_o \sqrt{H_o} T_o \sqrt{1-\lambda}}{H_o^{5/2} T_f} \quad (5c)$$

Thus (a) the height of the interface layer given by Eq.5b, together with (b) Eq.1 and the following relation for the plume temperature:

$$\frac{\Delta T_p}{T_a} Z_N^{\frac{5}{3}} = \text{constant (if flame height} < Z_N) \quad (6a)$$

allow the determination of the temperature in the upper layer i.e.:

$$\frac{\Delta T_f}{T_a} Z_N^{\frac{5}{3}} \propto (1 - \lambda) \quad (6b)$$

or after substitution from Eq.5b

$$\left(\frac{\Delta T_f}{T_a} \left(\frac{T_a}{T_f} \right)^{\frac{2}{3}} \right)^{\frac{3}{2}} \propto f_1 (1 - \lambda) \quad (6c)$$

where f_1 is a function of heat loss fraction λ . Prior to examining its value, it is important to make a modification of Eq.6c if the flame height from the pan fire is larger than the interface height Z_N .

$$\frac{\frac{\Delta T_f \left(\frac{T_o}{T_f} \right)^{2/3}}{T_a \left(\frac{T_o}{T_f} \right)} = f_1(1-\lambda) f_2 \left(\frac{Z_N}{L_f} \right)}{\left(\frac{\dot{Q}}{A_o \sqrt{H_o}} \right)^{2/3}} \quad (7a)$$

By using Eq.5b (and neglecting $(T_o/T_f)^{2/5}$ and the heat loss fraction) and setting also $L_f \propto Q^{2/5}$

$$\frac{Z_N}{L_f} \propto \frac{\left(A_o \sqrt{H_o} \right)^{2/5}}{\dot{Q}^{2/5}} \quad (7b)$$

The final result is general form like:

$$\frac{\frac{\Delta T_f \left(\frac{T_o}{T_f} \right)^{2/3}}{T_a \left(\frac{T_o}{T_f} \right)} = f \left(\lambda, \frac{\left(A_o \sqrt{H_o} \right)^{2/5}}{\dot{Q}^{2/5}} \right)}{\left(\frac{\dot{Q}}{A_o \sqrt{H_o}} \right)^{2/3}} \quad (7c)$$

By assuming that (a) the heat transfer is proportional to the product of the plume velocity and its temperature (b) the wall temperature is approximately the initial temperature (c) the enclosures are geometrically similar it can be shown that the heat loss fraction is a function of Z_N/H .

$$\lambda = \text{fcn} \left(\frac{Z_N}{H} \right) \approx \text{fcn} \left(\frac{\left(A_o \sqrt{H_o} \right)^{2/5}}{H} \right)$$

(7d)

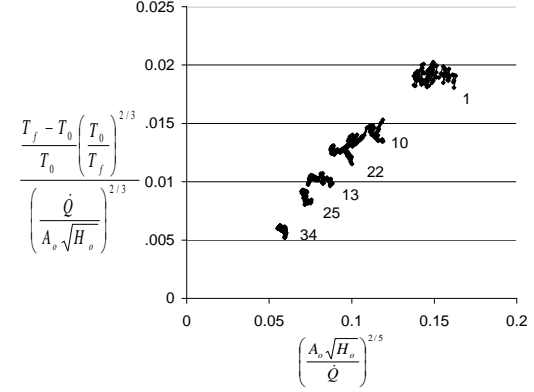
where H is the height of the enclosure. Thus the final formula for the gas is:

$$\frac{\frac{\Delta T_f \left(\frac{T_o}{T_f} \right)^{2/3}}{T_a \left(\frac{T_o}{T_f} \right)} = \text{fcn} \left(\frac{\left(A_o \sqrt{H_o} \right)^{2/5}}{\dot{Q}^{2/5}}, \frac{\left(A_o \sqrt{H_o} \right)^{2/5}}{H} \right)}{\left(\frac{\dot{Q}}{A_o \sqrt{H_o}} \right)^{2/3}} \quad (8)$$

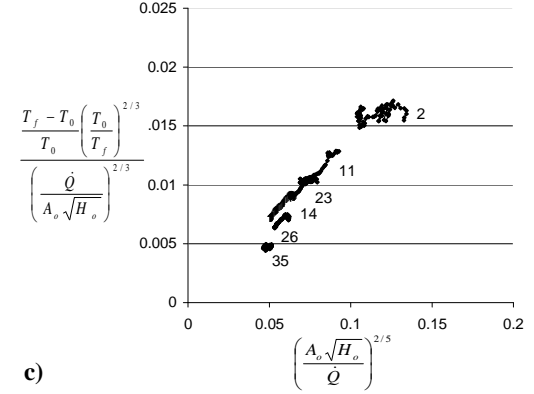
This relation is examined by plotting the experimental data from this project in Figs. 13a for the small, 13b for the medium and 13c for the large pan size and the fire located in the center of the enclosure and

Figs. 14a, 14b and 14c respectively for the fire located in the corner of the enclosure.

a)



b)



c)

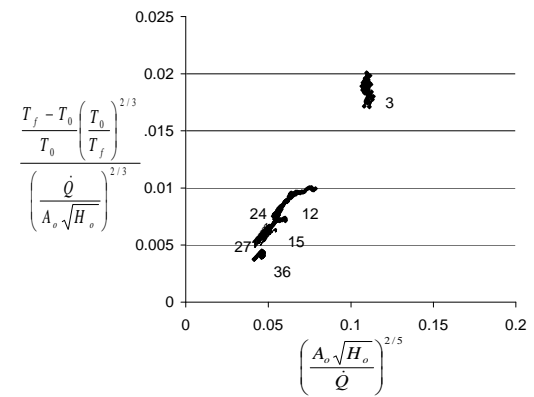


Figure 13 (a,b,c) Centre fires. Normalized gas temperature versus the ratio of the opening length scale ($\sim A_o \sqrt{H_o}^{2/5}$) to the flame height length scale ($\sim \dot{Q}^{2/5}$) with an additional parameter the ratio of the opening length scale to the enclosure height.

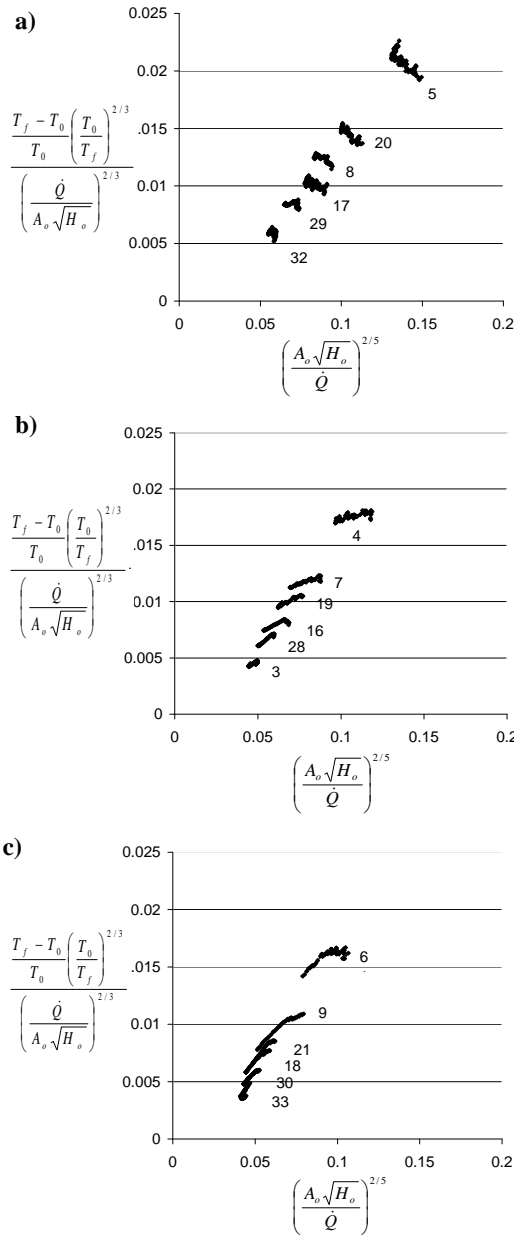


Figure 14 a,b,c. Corner fires. Normalized gas temperature versus the ratio of the opening length scale ($\sim A_o \sqrt{H_o}$)^{2/5} to the flame height length scale ($\sim \dot{Q}^{2/5}$) with an additional parameter the ratio of the opening length scale to the enclosure height

The correlation of the data is apparently good but more analysis and discussion is needed and will be presented in a separate paper. Suffice to say that there are two independent dimensionless parameters (see Eq.8) that control the gas temperature in an enclosure a) the ratio of an opening length scale $(A_o \sqrt{H_o})^{2/5}$ to a flame height scale $(\dot{Q}^{2/5})$ and (b) the ratio of the same opening length scale to the height of the enclosure. The former parameter characterizes the variation of entrainment to the plume as the flame height reaches or exceeds the neutral (smoke) layer height; whereas, the latter parameter characterizes the magnitude of the heat losses to the boundaries which increase as this parameter decreases (namely, as the neutral plane level approaches the bottom of the opening).

The heat release rate in the previous correlations is calculated by multiplying the measured mass loss rate by the theoretical heat of combustion. This approach neglects, on the one hand, the inefficiency of combustion when the fire is well ventilated and on the other hand, the partial combustion of the fuel when the fire is under ventilated. Both these approximations would not change significantly the proposed correlations.

5. Conclusions

This work being part of continuing effort at FireSERT [3,4,8,9] to measure and model fires in enclosures yields the following conclusions:

1. A new heat flux gauge (Figs.3 and 4) enables the determination of the distribution of the heat flux on a wall of an enclosure. In combination with a Gardon gauge at selected positions, it

- determines also the heat transfer coefficient for convection.
2. The previously found [3,4] dependence of the normalized mass loss rate on the normalized opening factor (see Fig.8a) must be modified to account for low gas temperatures inside the enclosure (see Fig.8b).
 3. The heat fluxes to the wall depend on the local gas temperature (see Figs. 9a, 10a and Figs. 9b, 10b) if the flame radiation from the fire is not significant (see Figs 9c, 10c).
 4. The gas temperature of the hot layer inside the enclosure is correlated with the size of the opening and the intensity of the fire using a new approach different from the MQH correlation [1,2]. This approach includes the modification of both the entrainment if the flame height is greater than the smoke interface height and the heat losses to the boundaries of the enclosure.
7. Wickstrom, U., "The Plate thermometer – a simple instrument for reaching harmonized fire resistance test", NORDTEST project 609.86, SP Report 1989:03, Swedish National Testing Institute Fire Technology, Boras 1988
 8. Shields, T.J., Silcock, G.W.H., and Flood, F., "Performance of a Single Glazing Assembly Exposed to Enclosure Corner Fires of Increasing Severity", *Fire and Materials*, 25, 123-152, 2001
 9. Shields, T.J., Silcock, G.W.H., and Flood, F., "Performance of a Single Glazing Assembly Exposed to a Fire in the Centre of an Enclosure", *Fire and Materials*, 26, 51-75, 2002

References

1. Drysdale, D.D., *An Introduction to Fire Dynamics*, Wiley, 1990.
2. Karlsson, B., Quintiere J.G, *Enclosure Fire dynamics*. CRC Press.
3. Delichatsios et al, Mass pyrolysis rates and excess pyrolysate in fully developed enclosure fires, *Fire Safety Journal*, Volume 39, Issue 1, Pages 1-21
4. Delichatsios MA, Silcock GWH. Fully developed enclosure fires: effects of fuel type, fuel area and enclosure geometry. Invited Lecture at the 7th IAFSS Symposium on combustion, June 2002
5. Design and calibration of new heat flux probe. Interim report , FireSERT 2004 (available on request).
6. Ingason, H. And de Ris, J., "Flame Heat Transfer in Storage Geometries"